Journal of Environmental Chemical Engineering 10 (2022) 108011

Contents lists available at ScienceDirect

Journal of Environmental Chemical Engineering

journal homepage: www.elsevier.com/locate/jece

# Catalytic membrane reactor based on Pd-Sn supported on nanocarbons for the reduction of nitrate in water

A. Marí, J.A. Baeza *, L. Calvo, M.A. Gilarranz

*Departamento de Ingeniería Química, Universidad Autónoma de Madrid, C/Francisco Tomás y Valiente 7, 28049 Madrid, Spain*

ARTICLE INFO

Editor: Apostolos Giannis

*Keywords:*
Carbon
Catalytic membranes
Flow-through configuration
$NO_3^-$ reduction
Mass transfer limitations
Pd-Cu catalysts
Pd-Sn catalysts

ABSTRACT

This work studies the reduction of $NO_3^-$ in water using a catalytic membrane reactor in flow-through configuration (FTCMR) for enhanced control of $H_2$ availability and generation of $NH_4^+$. The catalytic membrane was prepared with metal catalysts supported on carbon materials with different structural and physicochemical properties (graphite, carbon nanofibers, reduced graphene oxide, activated carbon and carbon black). The catalysts were firstly tested in a batch reactor for screening and assessing influence of regime control on activity and selectivity. Pd-Sn catalysts showed higher production of $NH_4^+$ under chemical control than Pd-Cu ones, but equivalent performance was reached for Pd-Sn supported on carbon nanofibers and carbon black in conditions of $H_2$ mass transfer control. Catalytic membranes were prepared with Pd-Sn catalyst according to higher impact of $H_2$ availability in $NH_4^+$ generation. FTCMR was less selective to $NH_4^+$ compared to the batch reactor due to better control of $H_2$ mass transfer. Reduction of $NH_4^+$ generation was achieved at the expense of activity due to lower availability of $H_2$. However, membranes based on Pd-Sn supported on carbon nanofibers and carbon black were able to operate at higher $H_2$ concentration with low selectivity to $NH_4^+$, making possible the use of membrane reactors at advantageous conditions.

## 1. Introduction

Water pollution by $NO_3^-$ represents an important issue for human health and the environment. $NO_3^-$ is reduced to $NO_2^-$ in the human body, being a precursor of carcinogenic nitrosamines and the cause of blue-baby syndrome. Moreover, $NO_3^-$ is also responsible for the eutrophication of rivers and lakes [1]. $NO_3^-$ is released to water from multiple sources, including fertilizers, manure, soil, urban sewage and industrial effluents. Dissolved N-compounds percolate soil, reaching groundwater and causing pollution [2]. Currently, catalytic reduction via hydrogenation over noble-metal catalysts stands out for being an effective technique for water denitrification. This process was firstly described by Vorlop et al. [3]. It was reported that the first step in $NO_3^-$ reduction is the conversion to $NO_2^-$. Then, $NO_2^-$ is reduced to $N_2$ or the undesired $NH_4^+$ according to the following reaction scheme [4]:

$$2\ NO_3^- + 2\ H_2 \xrightarrow{Pd-Cu} 2\ NO_2^- + 2\ H_2O$$

$$2\ NO_2^- + 3\ H_2 \xrightarrow{Pd} N_2 + 2\ H_2O + 2\ OH^-$$

$$2\ NO_2^- + 6\ H_2 \xrightarrow{Pd} 2\ NH_4^+ + 4\ OH^-$$

In most of the studies on $NO_3^-$ catalytic reduction, $NH_4^+$ concentration reaches values above standards in legislation. Therefore, the development of new strategies to reduce selectivity to $NH_4^+$ is still a challenge. European legislation (98/83/CE) has established the limit concentrations for $NO_3^-$, $NO_2^-$ and $NH_4^+$ at 50, 0.1 and 0.5 mg/L, respectively, in water for human consumption [5,6]. World Health Organisation (WHO) recommended concentrations of 50 and 3 of $NO_3^-$, $NO_2^-$ mg/L, respectively, and a $NH_4^+$ suggested taste threshold of 35 mg/L [7].

Since successful $NO_3^-$ reduction was first reported using a Pd-Cu catalyst [3], numerous studies using bimetallic catalysts have been published. In them, metallic phases are commonly composed by Pd, Pt or Rh as noble metal and transition/post transition metals (M) such as Cu, Sn, In or Ni as a promoter, which enhances the conversion of $NO_3^-$ to $NO_2^-$ by promoting the redox cycle involving the noble metal and $H_2$. Moreover, a variety of materials, such as alumina, silica, ceria, titania or activated carbon (AC) have been used as supports [8–14]. Pd is the noble metal leading to better reported results, with Pd-Cu, Pd-Sn and Pd-In as the bimetallic pairs achieving the best performances in the catalytic reduction of $NO_3^-$ [15]. Different studies have been carried out to

* Corresponding author.
*E-mail address:* josealberto.baeza@uam.es (J.A. Baeza).

https://doi.org/10.1016/j.jece.2022.108011
Received 3 February 2022; Received in revised form 9 May 2022; Accepted 29 May 2022
Available online 2 June 2022
2213-3437/© 2022 The Author(s). Published by Elsevier Ltd. This is an open access article under the CC BY-NC-ND license (http://creativecommons.org/licenses/by-nc-nd/4.0/).

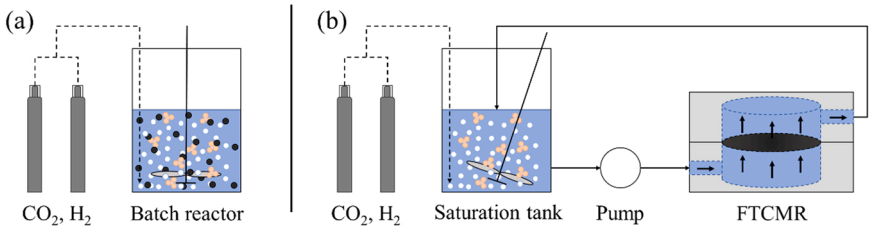


**Fig. 1.** Scheme of (a) batch reactor and (b) FTCMR systems.

compare Cu and Sn as promoting metals, but no clear trends have been observed in terms of activity or selectivity to $NH_4^+$, although Pd-Sn have been found to be less prone to leaching. The discrepancies in literature may result from the role that the support, the reaction medium and the type of reactor have in catalysts performance. Pintar et al. [16] reported that Pd-Cu catalysts supported on alumina spheres had higher activity and less selectivity to $NH_4^+$ than Pd-Sn catalysts in the reduction of $NO_3^-$ in synthetic waters. However, other authors reported that Pd-Sn catalyst supported on alumina had higher activity and lower selectivity to $NH_4^+$ in the reduction of $NO_3^-$ in natural groundwater because this metallic pair was less affected by water conductivity and hardness [17,18]. Lemaignen et al. [19] assayed the reduction of $NO_3^-$ in synthetic water using Pd-Cu/AC and Pd-Sn/AC catalysts in semi-batch stirred reactor and achieved higher reaction rates for Pd-Cu/AC catalyst, but similar $NH_4^+$ production for both catalysts. On the other hand, Yuranova et al. [20] reported that high catalytic activity was observed for both Pd-Cu and Pd-Sn nanoparticles working in semi-batch and continuous reactor, but lower selectivity to $NH_4^+$ was achieved for the Pd-Sn catalysts, especially when supported on carbon nanofibers (CNF).

In the last years, catalytic membrane reactors (CMR) have been developed as an alternative to conventional reactors, such as batch or fixed beds. They can overcome transport limitations, which in the reduction of $NO_3^-$ is an important aspect due to the low solubility and accessibility of $H_2$ to the catalyst surface [15]. CMR in flow-through configuration (FTCMR), where the liquid phase is first saturated in $H_2$ and then pumped through the catalytic membrane, and CMR in interfacial configuration, where the gas/liquid interface is located inside the catalytic membrane, have been proven to achieve the best $NO_3^-$ reduction rates. Ilinitch et al. [21] reported an improvement in $NO_3^-$ reduction when Pd-Cu/γ-$Al_2O_3$ membranes were used in flow-through configuration, suggesting that internal diffusion limitations were diminished. On the other hand, Chen et al. [22] reported that $NO_3^-$ conversion was enhanced when Pd-Cu/γ-$Al_2O_3$ particles were supported on tubular ceramic membranes and the reaction was carried out in interfacial configuration, ascribing this improvement to a better gas-liquid-solid contact.

In the present work, catalysts supported on carbon materials with different structural and physicochemical properties have been studied for $NO_3^-$ reduction in a membrane reactor with FTCMR configuration for enhanced control of $H_2$ at the catalyst. A study of $H_2$ mass transfer and its influence in activity and selectivity to $NH_4^+$ was conducted in a batch reactor with Pd-Sn catalysts and comparison to previous results with Pd-Cu pair was carried out to select the most suitable catalysts for catalytic membranes. The control of $H_2$ availability was explored as a strategy to limit the selectivity to $NH_4^+$ in the FTCMR.

## 2. Experimental

### 2.1. Materials

$PdCl_2$ (≥ 99.999%), $SnCl_2$ (≥ 99.99%), $NaHCO_3$ (≥ 99.5%), graphite powder < 20 μm (G), graphitized CNF and 2,6-Pyridinedicarboxylic acid (≥ 99.5%) were supplied by Sigma-Aldrich. Panreac provided $Na_2HCO_3$ (≥ 99.5%), $NaNO_2$ (≥ 99%), $NaNO_3$ (≥ 99%), $NH_4Cl$ (≥ 99.5%), HCl (37%) and $H_2SO_4$ (≥ 98%). Nippon gases supplied $H_2$ (≥ 99.999%) and $CO_2$ (≥ 99.99%). Reduced graphene oxide (rGO) was provided by Applynano Solutions S.L., AC by Norit and $HNO_3$ (≥ 65%) by Honeywell. Timcal supplied ENSACO250G (ENS250) and ENSACO350G (ENS350) carbon blacks.

### 2.2. Catalyst preparation and characterization

Bimetallic (5 wt%) catalysts with 2:1 Pd-Sn mass ratio were prepared by wet impregnation of G, CNF, rGO, AC ENS250 and ENS350. $PdCl_2$ and $SnCl_2$ were dissolved in 4 mL of 0.1 M HCl and stirred for 24 h at room temperature. Then, Pd solution was added to 1 g of carbon support and vacuum dried at 70 ºC, 150 mbar and 200 rpm. After that, it was dried at 60 ºC for 24 h. Then, Sn solution was impregnated, following the same methodology for drying. The catalyst was calcined in an oven at 200 ºC for 2 h with a 10 ºC/min ramp and reduced at 200 ºC, using 25 N mL/min of $H_2$ for 2 h.

Catalysts were characterized by X-ray Photoelectron Spectroscopy (XPS), X-Ray Diffraction (XRD) and Transmission Electron Microscope (TEM). Both, the extent of Pd and Sn reduction and oxidation state were characterized using XPS (K-Alpha Thermo Scientific equipped with an AlKα X-Ray excitation source, 1486.68 eV). Zerovalent and electrodeficient metal species were calculated from deconvoluted signals using XPSPEAK v4.1 software. Crystalline structure characterization was carried out by XRD (X-pert PRO Theta/2Theta from Panalytical). Characteristic peaks (002) and (100) were determined to calculate stacking height ($L_c$) and crystallite size ($L_a$) using Scherrer equation according to Eqs. 1 and 2, respectively:

$$L_c = \frac{K.\lambda}{FWHM.cos\theta} \quad (1)$$

Where $K$ is the Scherrer parameter (0.94), $\lambda$ is the X-Ray wavelength (0.154051 nm), *FWHM* (rad) is the full width at half maximum of the diffraction peak (002) and $\theta$ (rad) is the Bragg angle corresponding to the diffraction peak (002).

$$L_a = \frac{K.\lambda}{FWHM.cos\theta} \quad (2)$$

Where $K$ is the Scherrer parameter (1.84), $\lambda$ is the X-Ray wavelength (0.154051 nm), *FWHM* (rad) is the full width at half maximum of the diffraction peak (100) and $\theta$ (rad) is the Bragg angle corresponding to the diffraction peak (100). Support morphology and metal nanoparticle size were characterized by TEM (JEOL JEM 2100 with EDS from Oxford 99 instruments). 150–200 metal particles were counted from representative images to calculate mean nanoparticle size and standard deviation.

BET specific surface area ($SSA_{BET}$) and porosity were characterized for all the tested supports in a previous study [23]. AC (1210 $m^2/g$) and ENS350 (720 $m^2/g$) were the supports with highest surface area, followed by rGO (86 $m^2/g$) and ENS250 (65 $m^2/g$). CNF (4 $m^2/g$) and G (2 $m^2/g$) were the supports with lowest specific area. AC (0.38 $cm^3/g$), rGO (0.59 $cm^3/g$) and ENS350 (0.74 $cm^3/g$) were the supports with highest mesopore volume, in contrast to CNF (0.06 $cm^3/g$), G (0.04 $cm^3/g$) and ENS250 (0.09 $cm^3/g$). The supports with highest

**Table 1**
Reaction conditions and metal and pollutant concentrations.

| Reactor | Volume (mL) | $m_{catalyst}$ (mg) | $[NO_3^-]$ (mg/L) | $[M_{Pd\text{-}Sn}]$ (mg/L) | $[M_{Pd\text{-}Sn}]/[NO_3^-]$ |
|---|---|---|---|---|---|
| **Batch (1)** | 150 | 60 | 100 | 20 | 0.2 |
| **Batch (2)** | 150 | 60 | 20 | 20 | 1.0 |
| **FTCMR** | 60 | 60 | 30 | 50 | 1.7 |

micropore volume were AC (0.53 $cm^3/g$), rGO (0.12 $cm^3/g$) and ENS350 (0.12 $cm^3/g$). CNF (0.005 $cm^3/g$), G (0.003 $cm^3/g$) and ENS250 (< 0.001 $cm^3/g$) exhibited much lower microporosity.

Electrical conductivity was also characterized in a previous work [23] for all the supports tested: G (0.9 S/cm), CNF (3.6 S/cm), rGO (0.5 S/cm), AC (1.2 S/cm), ENS250 (0.9 S/cm) and ENS350 (4.8 S/Cm).

Carberry number for the study of gas-liquid ($Ca_{G\text{-}L}$) and liquid-solid ($Ca_{L\text{-}S}$) mass transfer and Weisz-Prater modules for the study of the internal intraparticle diffusion were calculated according to the methodology described in our previous work [23].

### 2.3. Catalytic runs

$NO_3^-$ reduction was carried out in two different reaction systems: batch reactor (Fig. 1a) and FTCMR (Fig. 1b) with recirculation from $H_2$ saturation tank. Experimental procedure in the batch reactor was described elsewhere [23]. Regarding the FTCMR, catalytic membranes 32 mm in diameter and containing 60 mg of catalyst were prepared from 1 g/L catalyst suspension, sonicated for 30 min and vacuum filtered in a 47 mm support (polypropylene, 0.22 μm pore size, Filter-Lab) to form the membrane. The FTCMR was 30 mm in diameter and 30 mm in length.

Catalytic reduction tests were performed at room temperature (25 ± 5 ºC) with 60 mL of a 30 mg/L $NO_3^-$ solution. A typical essay started with the solubilization of $H_2$ in 58.5 mL of pure water under 1–50 N mL/min of $H_2$ and 50 N mL/min $CO_2$ flow and stirring at 600 rpm for 30 min. Meanwhile, the FTCMR was assembled with the catalytic membrane supported on the mid-point of the cell. Subsequently, the FTCMR water was pumped from the $H_2$ solubilization tank to the FTCMR at 3.6 mL/min flow and recirculated to the $H_2$ solubilization tank again. Once the system was filled and gas retained was purged, a pulse of 1.5 mL of concentrated $NO_3^-$ solution was fed to the stirring tank ($t = 0$ min). Experiments were carried out for 4 h and successive samples (1.5 mL) were taken every hour.

Table 1 summarizes the experimental conditions: volume of reaction, pollutant concentration, metal (M) concentration and metal-pollutant ratios (w/w).

Ion chromatography (Metrohm 882 Compact IC plus anion and cation) was used to determine $NO_3^-$, $NO_2^-$ and $NH_4^+$ concentration throughout the catalytic runs. $NO_3^-$, $NO_2^-$ and other anions were separated using Metrosep A Supp 5 column and 0.7 mL/min of 1 mM $NaHCO_3$ and 3.7 mM $Na_2CO_3$ eluent. $NH_4^+$ and other cations were separated using a Metrosep C 6 column and 0.9 mL/min of 1.7 mM 2,6-Pyridinedicarboxylic acid and 1.7 mM $HNO_3$ eluent.

$NO_3^-$ conversion was calculated according to Eq. (3). Selectivity to $NO_2^-$ and $NH_4^+$ were calculated according to Eqs. (4) and (5), respectively:

$$X_{NO_3^-}(\%) = \frac{n_{NO_{3,\ t=0}^-} - n_{NO_{3,\ t}^-}}{n_{NO_{3,\ t=0}^-}} \cdot 100 \quad (3)$$

$$S_{NO_2^-}(\%) = \frac{n_{NO_{2,\ t}^-}}{n_{NO_{3,\ t=0}^-} - n_{NO_{3,\ t}^-}} \cdot 100 \quad (4)$$

$$S_{NH_4^+}(\%) = \frac{n_{NH_{4,\ t}^+}}{n_{NO_{3,\ t=0}^-} - n_{NO_{3,\ t}^-}} \cdot 100 \quad (5)$$

Where $n_{i,t=0}$ is the initial amount of compound $i$ (mol) and $n_{i,t}$ is the amount of compound $i$ (mol) at time $t$ (min).

## 3. Results and discussion

### 3.1. Support and catalyst characterization

TEM images showing the metallic phase dispersion and particle frequency histograms for the Pd-Sn catalysts tested are given in Fig. 2. Metallic nanoparticles mean size and standard deviation were in a range from 2.4 to 6.3 nm and 0.6–2.6 nm, respectively. Pd-Sn/G and Pd-Sn/rGO were the catalysts exhibiting the smaller nanoparticle mean size (< 3 nm) and greater particle dispersion, although the largest nanoparticles did not exceed 6 nm for those catalysts. Pd-Sn/AC, Pd-Sn/ENS250 and Pd-Sn/ENS350 were catalysts with intermediate nanoparticle mean size (from 3.1 to 4.7 nm). They exhibited good dispersion as well, although some nanoparticle agglomerations were observed. Pd-Sn/CNF was the catalyst with a largest nanoparticle mean size, with nanoparticle sizes up to 18 nm. Small agglomerations of metallic nanoparticles were observed as well for this catalyst.

Fig. 3 shows XRD diffraction spectra for three Pd-Sn/G, Pd-Sn/CNF and Pd-ENS250 representative catalysts and AC, ENS350 and rGO supports. A peak at 26º is observed in all the patterns, which corresponds to the (002) reflection plane of carbon and it is related to the stacking of aromatic layers [24,25]. Broad peaks may be attributed to the small size of the crystallites perpendicular to the aromatic layers in both rGO and ENS350 supports and Pd-Sn/ENS250 catalyst. In addition, 2θ angle is shifted to higher values as the carbon content and graphitization of the supports increase, being higher for G, CNF and AC. Another peak was exhibited at 42º, although in the diffractograms with very narrow and intense peaks at 26º it is barely visible. This peak corresponds to the reflection in the (100) plane of aromatic layers and is attributed to the degree of condensation of the aromatic rings, becoming narrower and higher as the size of the aromatic layer increases [25]. The peak at 40º corresponds to the (111) reflection plane of Pd [26,27].

$L_c$ and $L_a$ values for the catalysts tested are given in Table 2. $L_c$ value indicates the thickness of the stacked structure [24] and, in agreement with the XRD patterns previously discussed, G, CNF and AC were the carbon materials with higher stacking height as their diffraction patterns exhibited a very narrow and intense (002) peak. rGO, ENS250 and ENS350 showed relatively low stacking height and small crystallite size. G and CNF were the carbon supports with larger crystallite sizes.

XPS was used to determine the oxidation state of Pd and Sn in the Pd-Sn catalysts tested, spectra can be seen in supplementary material (Figure I and II, respectively). In Table 3, the zerovalent ($M^0$) and electro-deficient ($M^{n+}$) percentages of Pd and Sn in each catalyst are given. Deconvoluted peaks showed binding energies that can be attributed to metallic Pd ($Pd^0$) in the range from 335.6 to 335.9 eV for Pd $3d_{5/2}$ and 340.9–341.2 eV for Pd $3d_{3/2}$; to electro-deficient Pd ($Pd^{n+}$) in the range from 336.2 to 337.7 eV and 341.7–343.1 eV for Pd $3d_{5/2}$ and Pd $3d_{3/2}$, respectively; to metallic Sn ($Sn^0$) in the range from 485.2 to 486.5 eV for Sn $3d_{5/2}$ and from 493.7 to 495.4 eV for Sn $3d_{3/2}$; and to electro-deficient Sn ($Sn^{n+}$) in the range from 486.7 to 487.4 eV and 495.1–496.0 eV for Sn $3d_{5/2}$ and Sn $3d_{3/2}$, respectively. These data are in good agreement with data reported in NIST X-ray Photoelectron Spectroscopy Database [28]. Percentages of $Pd^0$ higher than 60% were observed for the Pd-Sn/G, Pd-Sn/CNF, Pd-Sn/ENS250 and Pd-Sn/ENS350 catalysts. A lower reduction degree of Pd-Sn/rGO and Pd-Sn/AC is noticeable, but no direct correlation with the properties or supports and metal phase can be assessed. Commonly reasons for high electro-deficient to zerovalent species ratios, such as small nanoparticle size (higher prevalence of low coordination sites) or/and high microporosity contribution as preferent nanoparticle allocation with mass transfer limitations do not apply to these catalysts. Regarding Sn, all the catalysts showed a lower reduction than for Pd in general, because transition metals species have lower reduction potential [29]. Thus,

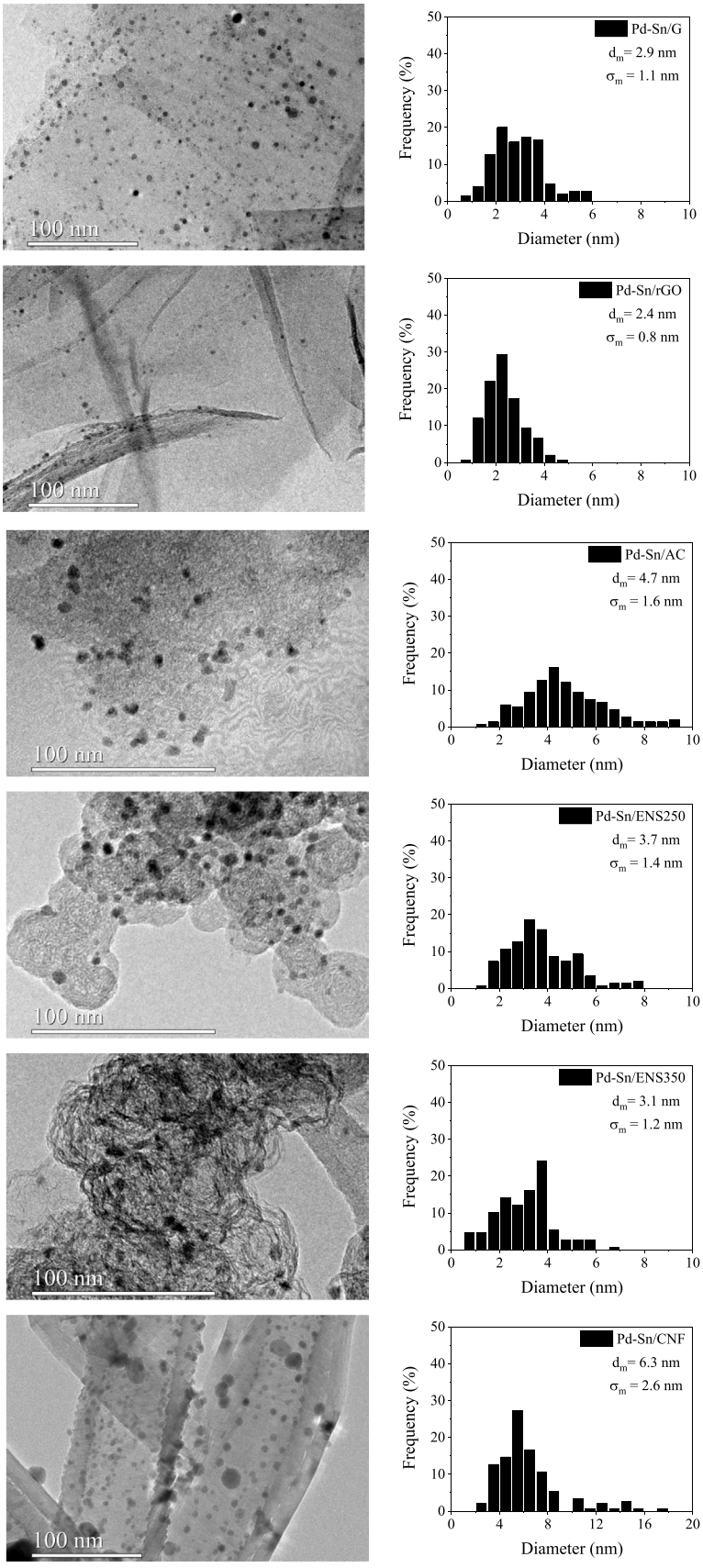


**Fig. 2.** TEM images and nanoparticle size histograms for the Pd-Sn catalysts tested.

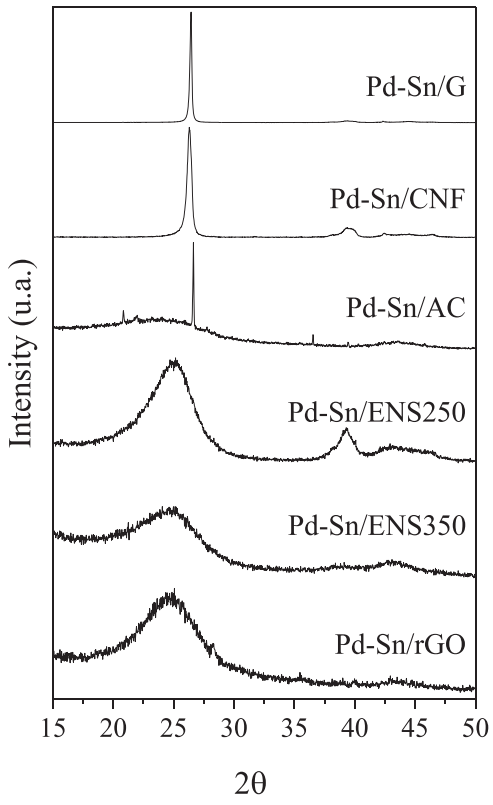


**Fig. 3.** X-ray diffractograms for the Pd-Sn catalysts tested.

**Table 2**
$L_c$ and $L_a$ values for the Pd-Sn catalysts tested.

| Catalyst | $L_c$ (nm) | $L_a$ (nm) |
|---|---|---|
| Pd-Sn/G | 42.7 | 102.8 |
| Pd-Sn/CNF | 19.9 | 43.9 |
| Pd-Sn/rGO | 1.4 | 3.1 |
| Pd-Sn/AC | 89.4 | 3.6 |
| Pd-Sn/ENS250 | 1.9 | 2.9 |
| Pd-Sn/ENS350 | 1.0 | 3.3 |

**Table 3**
Percentages $M^0$ and $M^{n+}$ for the Pd-Sn catalysts tested as determined by XPS.

| Catalyst | $Pd^0$ (%) | $Pd^{n+}$ (%) | $Sn^0$ (%) | $Sn^{n+}$ (%) | Pd/Sn (at/at%) | Pd/Sn (w/w %) |
|---|---|---|---|---|---|---|
| Pd-Sn/G | 72.9 | 27.1 | 11.5 | 88.5 | 62.8 | 60.2 |
| Pd-Sn/CNF | 92.5 | 7.5 | 29.9 | 70.1 | 60.6 | 58.0 |
| Pd-Sn/rGO | 42.1 | 57.9 | 15.7 | 84.3 | 52.9 | 50.1 |
| Pd-Sn/AC | 12.6 | 87.4 | 19.2 | 80.8 | 28.9 | 26.7 |
| Pd-Sn/ ENS250 | 77.9 | 22.1 | 20.9 | 79.1 | 53.6 | 50.8 |
| Pd-Sn/ ENS350 | 62.3 | 37.7 | 12.3 | 87.7 | 49.1 | 46.4 |

percentages of $Sn^0$ were in the range from 10% to 30% for all the catalysts studied. With regards to the Pd/Sn atomic and mass ratios on the catalyst surface, all the catalysts exhibited lower content of Pd than that expected from the nominal ratio (69.5% and 66.7%, respectively). This difference is mainly observed in the catalysts with high porosity, especially Pd-Sn/AC, suggesting preferent allocation of Pd metallic phase into pores. Pd-Sn/rGO, Pd-Sn/ENS250 and Pd-Sn/ENS350 also exhibited significant segregation of Pd but in a lower extent.

### 3.2. Reaction tests in batch reactor

Fig. 4 shows $NO_3^-$ conversion vs reaction time and selectivity to $NH_4^+$ vs $NO_3^-$ conversion for the Pd-Sn catalyst tested in the batch reactor. A wide activity range, from 40% to 100%, and selectivity to $NH_4^+$, from 15% to 70%, can be observed. Pd-Sn/AC, Pd-Sn/ENS250 and Pd-Sn/ENS350 were the most active catalysts, achieving complete conversion after 4 h of reaction. Partial conversion of $NO_3^-$ (< 70%) was achieved for the catalysts supported on CNF, G and rGO. Similar trends regarding the influence of the support were observed in a previous work [23] using Pd-Cu catalysts supported on carbon materials at the same reaction conditions. In general terms, the catalysts with higher surface area and more developed porosity (Pd-Sn/AC and Pd-Sn/ENS350) were found to exhibit higher activity, most probably because they allow for better dispersion of the metal phase [30–32]. However, Pd-Sn/ENS250 catalyst, which has both low specific surface area and micropore volume, showed similar activity and even better results in terms of $NH_4^+$ selectivity.

Pd-Sn/ENS250 was the catalyst with lower $NH_4^+$ production, while Pd-Sn/AC and Pd-Sn/ENS350 showed higher selectivity to $NH_4^+$ (> 50%). For the catalysts with lower activity (Pd-Sn/CNF, Pd-Sn/G and Pd-Sn/rGO), additional tests with a $NO_3^-$ initial concentration of 20 mg/L were carried out to study the selectivity at higher conversions. In these tests, Pd-Sn/CNF showed very low selectivity to $NH_4^+$, with a behaviour well differentiated from Pd-Sn/G and Pd-Sn/rGO. In general, the catalysts with higher microporosity led to greater production of $NH_4^+$ (Pd-Sn/AC, Pd-Sn/rGO and Pd-Sn/ENS350), in contrast with Pd-Sn/CNF and Pd-Sn/ENS250. In literature, this behaviour is ascribed to $OH^-$ mass transfer limitations from the micropores to the bulk solution that hinder their neutralisation in the acidified medium [33,34].

In our previous work based on Pd-Cu catalysts supported on carbon materials [23], a lower selectivity to $NH_4^+$ was also ascribed to higher conductivity of supports due to better charge transfer from metal to support. However, although similar trends were observed, Pd-Sn catalysts showed a higher production of $NH_4^+$. It has to be noted that Pd-Sn catalysts show in general terms smaller nanoparticles, resulting in higher prevalence of low coordination atoms [35,36]. Yoshinaga et al. [37] reported that low coordination sites such as edges or corners promote the hydrogenation of $NO_2^-$ increasing $NH_4^+$ production, whereas in terraces sites mild hydrogenation is produced. Chinthaginjala et al. [35] also concluded that selectivity to $NH_4^+$ in the reduction of $NO_2^-$ increased when metallic Pd particle sizes were decreased. However, in the current work, catalysts with larger nanoparticles (Pd-Sn/AC and Pd-Sn/ENS350) showed higher selectivity to $NH_4^+$, suggesting that over-reduction is favoured when bimetallic pair Pd-Sn is used.

In the literature, no conclusive results have been found enabling $NH_4^+$ selectivity comparison for Pd-Cu and Pd-Sn pairs. Al Bahri et al. [38] reported that Cu was the most adequate promoting metal when selectivity to $NH_4^+$ was considered for Pd-M catalysts supported on AC. Chollier-Brym et al. [39] also reported Pd-Cu catalyst was more active and less selective to $NH_4^+$ than Pd-Sn catalyst when supported on zirconia. On the other hand, Pizarro et al. [40] reported in their study higher conversion and lower selectivity to $NH_4^+$ for the Pd-Sn and Pd-In catalysts supported on pillared-clays.

The diversity of trends in literature may be related to the role of the support in some of the catalysts studied, which may comprise both activity and mass transfer. To address these effects, batch tests were carried out reducing $H_2$ flow in batch reactor. $CO_2$ flow was maintained at 50 N mL/min, which results in lower availably of $H_2$ due to lower partial pressure. The results for Pd-Sn/CNF, Pd-Sn/rGO, Pd-Sn/ENS250 and Pd-Sn/ENS350 can be observed in Fig. 5. The catalysts exhibited different behaviour although catalytic activity was decreased as a general trend when $H_2$ flow was reduced from 50 to 1 N mL/min. This trend was particularly evident in the case of Pd-Sn/rGO and Pd-Sn/ENS250 catalysts. However, in the case of Pd-Sn/ENS350 the decrease in activity was very low and for Pd-Sn/CNF it was not clearly observed until $H_2$ flow

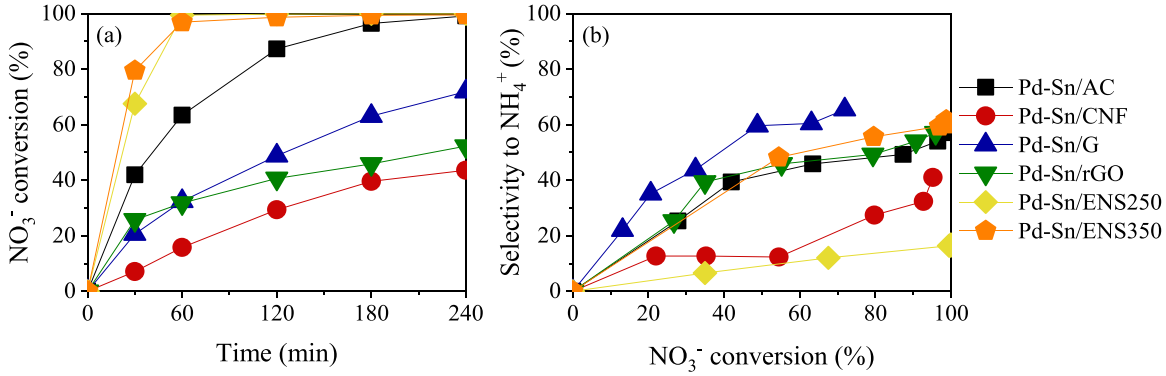


**Fig. 4.** Batch reactor tests at $[NO_3^-]_0 = 100$ mg/L for the Pd-Sn catalysts tested: (a) $NO_3^-$ conversion vs reaction time and (b) selectivity to $NH_4^+$ vs $NO_3^-$ conversion at $[NO_3^-]_0 = 20$ mg/L for Pd-Sn/CNF, Pd-Sn/G and Pd-Sn/rGO ($H_2$ flow = 50 N mL/min, $CO_2$ flow = 50 N mL/min, 0.4 g/L catalyst).

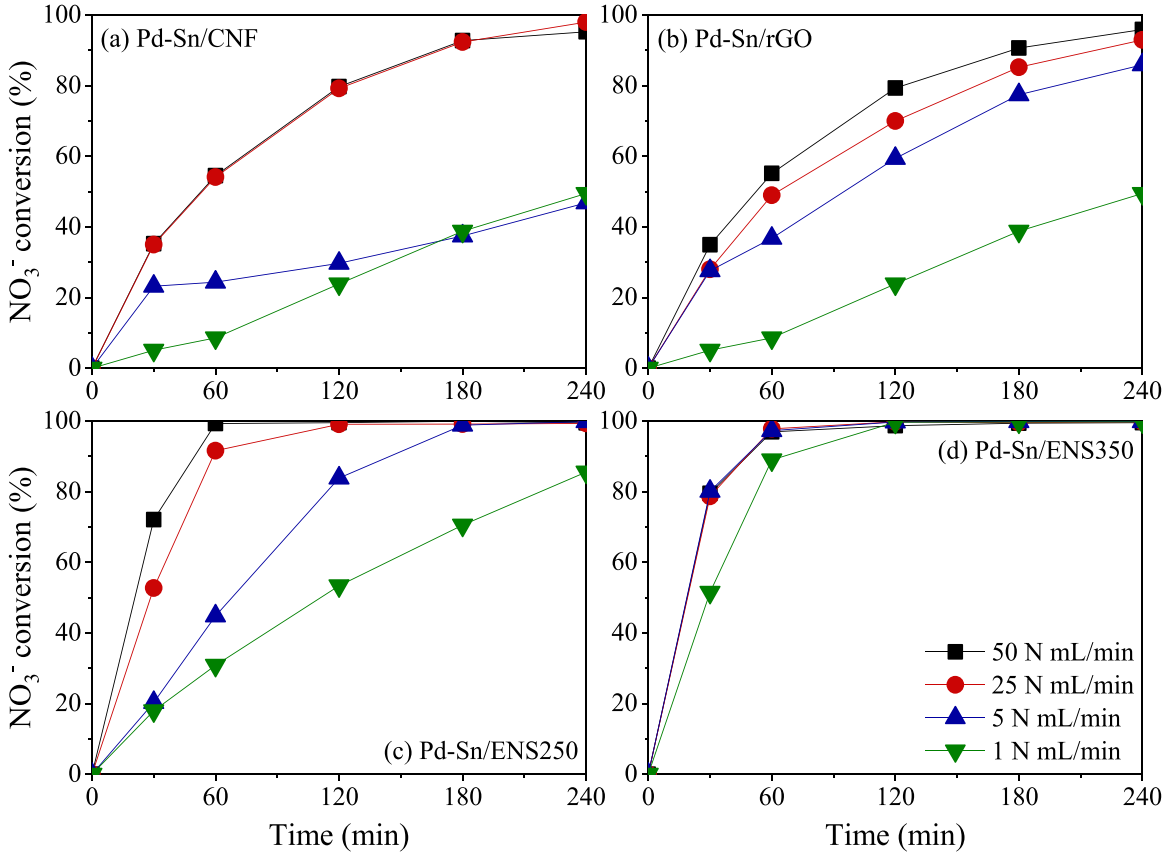


**Fig. 5.** $NO_3^-$ conversion vs reaction time for the (a) Pd-Sn/CNF, (b) Pd-Sn/rGO, (c) Pd-Sn/ENS250 and (d) Pd-Sn/ENS350 catalysts in batch reactor at different $H_2$ flows ($[NO_3^-]_0 = 20$ mg/L for Pd-Sn/CNF and Pd-Sn/rGO, $[NO_3^-]_0 = 100$ mg/L for Pd-Sn/ENS250 and Pd-Sn/ENS350, $CO_2$ flow = 50 N mL/min, 0.4 g/L of catalyst).

was reduced to 5 N mL/min. The structure these catalysts seems to favour $H_2$ transport, making them less sensitive to the decrease in flow.

The decrease in $H_2$ flow also resulted in an important reduction in selectivity to $NH_4^+$ (Fig. 6), which can be related to the lower availability of $H_2$, diminishing the H/N ratio and thus limiting the over-reduction of N-species to $NH_4^+$. Therefore, availability of $H_2$ together with the structure of the catalyst support is relevant for activity and selectivity and can lead to substantially different results for a given bimetallic pair. This may be one of the reasons for the disparity of results in relation to the comparison of Pd-Sn and Pd-Cu pairs behaviour. The direct comparison of Pd-Sn and Pd-Cu pairs for batch reactions at low $H_2$ flow can be found in supplementary material (Figure III, IV, V and VI). As a general trend, Pd-Cu catalysts exhibit a lower selectivity to $NH_4^+$ than Pd-Sn ones. However, for Pd-Sn-ENS250 and Pd-Sn-CNF the sensitivities to $H_2$ flow is higher and show a selectivity to $NH_4^+$ very close to Pd-Cu catalysts at low $H_2$ flows, even lower in the case of Pd-Sn/CNF.

A mass transfer regime study was conducted to assess control regime in the batch reactions at $H_2$ flow, being the results in terms of Carberry number and Weisz-Prater module given in Table 4. According to the criterion stablished by Carberry et al. [41], mass transfer limitations cannot be ruled out when $Ca > 0.05$. This is the case for $Ca_{G\text{-}L}$ in reactions with Pd-Sn/ENS250 and Pd-Sn/ENS350 when $H_2$ flow is lower than 25 N mL/min and Pd-Sn/CNF at the lowest $H_2$ flow (1 N mL/min). In addition, $Ca_{G\text{-}L}$ values close to the limit were observed for Pd-Sn/ENS250 and Pd-Sn/ENS350 (0.043 and 0.029) at 50 N mL/min and for Pd-Sn/CNF at 5 N mL/min. In these cases, mass transfer could

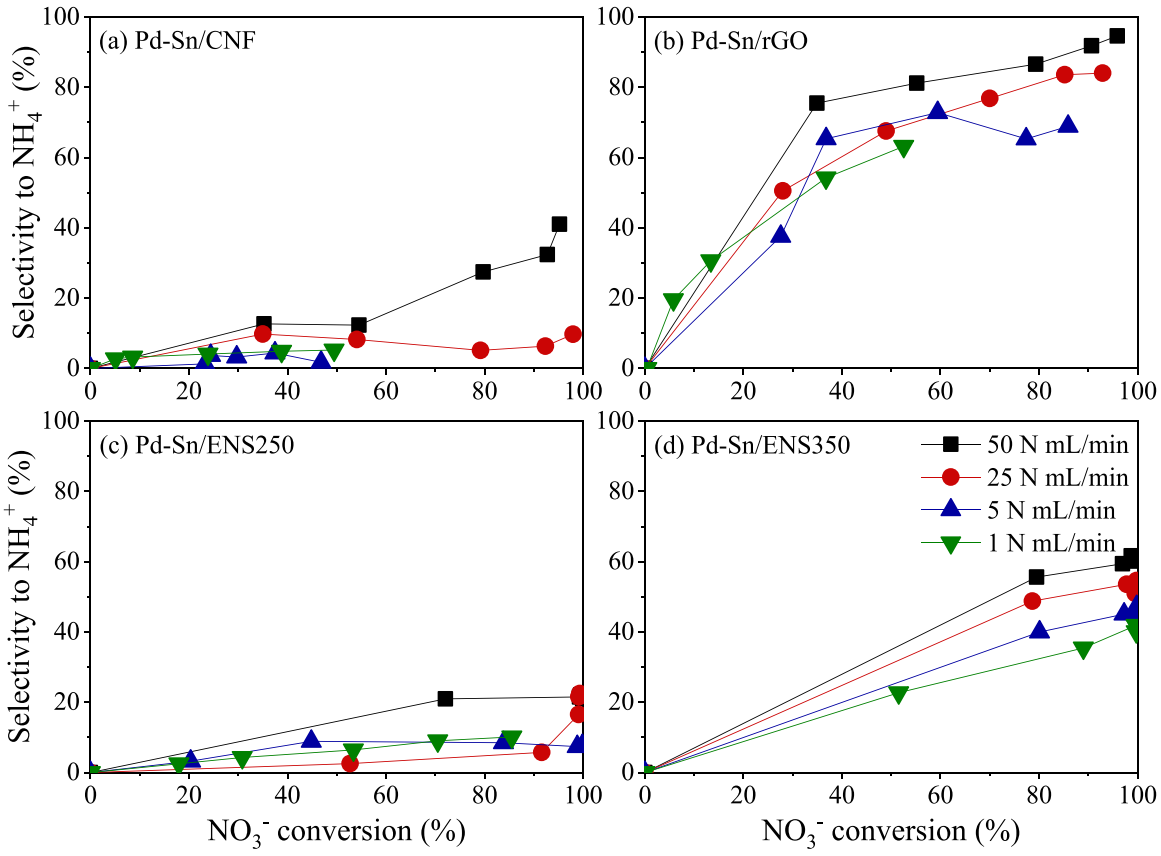


**Fig. 6.** Selectivity to $NH_4^+$ vs $NO_3^-$ conversion for the (a) Pd-Sn/CNF, (b) Pd-Sn/rGO, (c) Pd-Sn/ENS250 and (d) Pd-Sn/ENS350 catalysts in batch reactor at different $H_2$ flows ($[NO_3^-]_0$ = 20 mg/L for Pd-Sn/CNF and Pd-Sn/rGO, $[NO_3^-]_0$ = 100 mg/L for Pd-Sn/ENS250 and Pd-Sn/ENS350, $CO_2$ flow = 50 N mL/min, 0.4 g/L of catalyst).

**Table 4**
$Ca_{G\text{-}L}$, $Ca_{L\text{-}S}$, $(\Phi_s)_{H_2}$ and $(\Phi_s)_{NO_3^-}$ for the Pd-Sn/CNF, Pd-Sn/rGO, Pd-Sn/ENS250 and Pd-Sn/ENS350 catalysts at different $H_2$ flows.

| *Catalyst* | Flow (N mL/min) | $Ca_{G\text{-}L}$ ($\cdot 10^{-2}$) | $Ca_{L\text{-}S,\ H2}$ ($\cdot 10^{-6}$) | $Ca_{L\text{-}S,\ NO3\text{-}}$ ($\cdot 10^{-7}$) | $(\Phi_S)_{H2}$ ($\cdot 10^{-4}$) | $(\Phi_S)_{NO3\text{-}}$ ($\cdot 10^{-4}$) |
|---|---|---|---|---|---|---|
| *Pd-Sn/CNF* | 50 | 0.46 | 0.12 | 1.93 | 0.88 | 1.60 |
| | 25 | 0.83 | 0.18 | 1.92 | 1.31 | 1.59 |
| | 5 | 2.15 | 0.30 | 0.86 | 2.15 | 0.71 |
| | 1 | 5.90 | 0.52 | 0.30 | 3.76 | 0.25 |
| *Pd-Sn/rGO* | 50 | 0.47 | 0.12 | 1.96 | 0.89 | 1.62 |
| | 25 | 0.73 | 0.16 | 1.74 | 1.14 | 1.44 |
| | 5 | 2.93 | 0.40 | 1.30 | 2.94 | 1.08 |
| | 1 | 3.94 | 0.35 | 0.20 | 2.51 | 0.17 |
| *Pd-Sn/ENS250* | 50 | 4.27 | 1.12 | 3.53 | 8.15 | 2.92 |
| | 25 | 7.13 | 1.55 | 3.25 | 11.2 | 2.69 |
| | 5 | 20.0 | 2.76 | 1.59 | 20.0 | 1.31 |
| | 1 | 97.9 | 8.61 | 1.09 | 62.5 | 0.90 |
| *Pd-Sn/ENS350* | 50 | 2.90 | 0.76 | 2.53 | 5.53 | 2.09 |
| | 25 | 6.71 | 1.45 | 3.47 | 10.5 | 2.87 |
| | 5 | 40.0 | 5.53 | 3.45 | 40.1 | 2.85 |
| | 1 | 264 | 23.2 | 3.16 | 168 | 2.61 |

not be rigorously ruled out because of the proximity of the estimated values obtained to the limit of the Carberry criterion. Therefore, reduction of activity and selectivity to $NH_4^+$ could be ascribed to external gas-liquid mass transfer limitations and lower availability of $H_2$. Regarding $Ca_{L\text{-}S}$ and Weisz-Prater modules, calculated values did not show external liquid-gas mass transfer nor internal intraparticle diffusion constraints. The experiments at low $H_2$ flow achieving mass transfer control are indicative of the high potential of Pd-Sn catalysts, particularly Pd-Sn/CNF in reaction systems where $H_2$ availability is controlled.

### 3.3. Reaction tests in FTCMR

Enhanced control of $H_2$ availability was addressed by means of the FTCMR reaction system (Fig. 1b). In addition to the control of $H_2$ concentration in the saturation tank, concentration gradients across the catalytic membrane are minimized and gas- solid transport due to deficient wetting is avoided. Different consistency of the membranes was observed depending on the carbon support used. Thus, poor consistency was observed for Pd-Sn/CNF and Pd-Sn/rGO membranes. On the other hand, Pd-Sn/ENS350 membranes showed an uneven covering of the support. Membranes formed by Pd-Sn/AC, Pd-Sn/G and Pd-Sn/ENS250 showed a homogeneous covering and mechanical stability.

Fig. 7 shows $NO_3^-$ conversion vs reaction time and selectivity to $NH_4^+$ vs $NO_3^-$ conversion for Pd-Sn catalysts tested in the FTCMR. In terms of activity, similar behaviour was observed for all the catalysts, achieving complete $NO_3^-$ reduction after 4 h of reaction, but the reaction rate was especially higher for those which exhibited better performance in terms of membrane formation (Pd-Sn/AC, Pd-Sn/G and Pd-Sn/ENS250) probably because channelling is avoided. With regards to selectivity to $NH_4^+$, a wide range of values was observed (from 15% to 95%) at complete $NO_3^-$ conversion. Low production of $NH_4^+$ was observed for catalysts supported on CNF and ENS250 (< 20%), followed by AC and CB350G (< 40%). Higher $NH_4^+$ production was observed for G and especially for rGO (close to 100%). These results may support the importance of nanoparticle size in $NH_4^+$ selectivity, as it was previously discussed. It was also observed that catalysts supported on carbon materials with high or moderate electrical conductivity exhibited lower selectivity to $NH_4^+$ (Pd-Sn/CNF, Pd-Sn/AC and Pd-Sn/ENS350).

Although direct comparison between the batch reactor and FTCMR cannot be carried out strictly due to evident differences between both

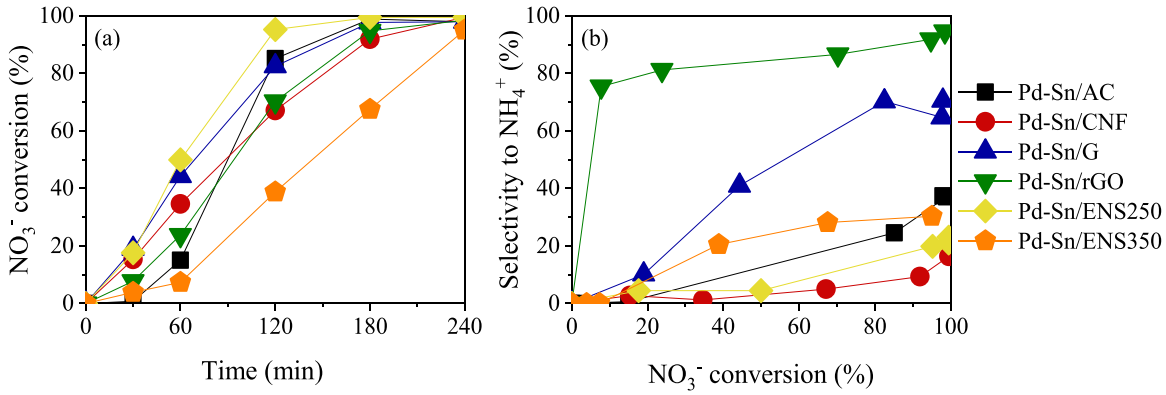


**Fig. 7.** FTCMR tests at $[NO_3^-]_0 = 30$ mg/L for the Pd-Sn catalysts tested: (a) $NO_3^-$ conversion vs reaction time and (b) selectivity to $NH_4^+$ vs $NO_3^-$ conversion ($H_2$ flow = 50 N mL/min, $CO_2$ flow = 50 N mL/min, 60 mg of catalyst, 30 mm in diameter FTCMR).

**Table 5**
Selectivity to $NH_4^+$ at 70% conversion rate for slurry and FTCMR reaction systems.

| Catalyst | Slurry | | FTCMR | |
|---|---|---|---|---|
| | **$[M_{Pd}\text{-}Sn]$ / $[NO_3^-]$** | **Selectivity to $NH_4^+$ (%)** | **$[M_{Pd}\text{-}Sn]$ / $[NO_3^-]$** | **Selectivity to $NH_4^+$ (%)** |
| **Pd-Sn/G** | 1.0 | 65 | 1.7 | 60 |
| **Pd-Sn/CNF** | 1.0 | 25 | 1.7 | 5 |
| **Pd-Sn/rGO** | 1.0 | 45 | 1.7 | 90 |
| **Pd-Sn/AC** | 0.2 | 45 | 1.7 | 20 |
| **Pd-Sn/ENS250** | 0.2 | 12 | 1.7 | 10 |
| **Pd-Sn/ENS350** | 0.2 | 50 | 1.7 | 30 |

reaction systems, lower selectivity to $NH_4^+$ was observed for catalysts supported on CNF, AC and ENS350 in FTCMR despite the fact that higher $M/NO_3^-$ ratio was used (Table 5), which may lead to enhanced hydrogenation of N-species promoting the over-reduction to $NH_4^+$. The lower production of $NH_4^+$ may be due to a better control of the $H_2$ reaching the catalytic sites.

Fig. 8 shows $NO_3^-$ conversion vs reaction time for the Pd-Sn/CNF, Pd-Sn/G, Pd-Sn/rGO and Pd-Sn/ENS250 catalysts in the FTCMR system for experiments carried out using $H_2$ flows of 50, 25 and 10 N mL/min, which resulted in estimated hydrogen concentration in water of 0.78, 0.52 and 0.26 mg/L, respectively. Complete conversion after 4 h of reaction was achieved for Pd-Sn/CNF, Pd-Sn/G and Pd-Sn/ENS250 catalysts when 25 and 50 N mL/min of $H_2$ were used, showing a low decrease of activity and suggesting shift to mass transfer control.

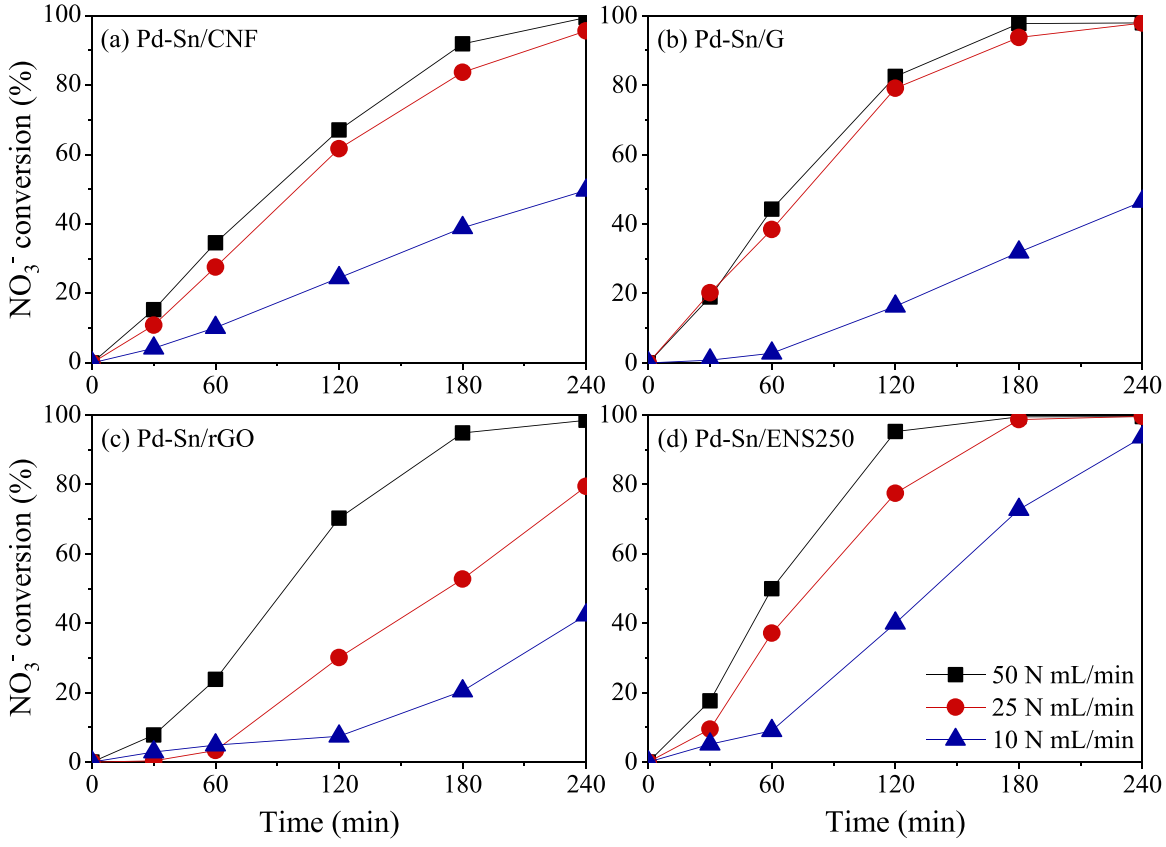


**Fig. 8.** $NO_3^-$ conversion vs reaction time for the (a) Pd-Sn/CNF, (b) Pd-Sn/G, (c) Pd-Sn/rGO and (d) Pd-Sn/ENS250 catalysts in FTCMR at different $H_2$ flows ($[NO_3^-]_0$ = 30 mg/L, $CO_2$ flow = 50 N mL/min, 60 mg of catalyst, 30 mm in diameter FTCMR).

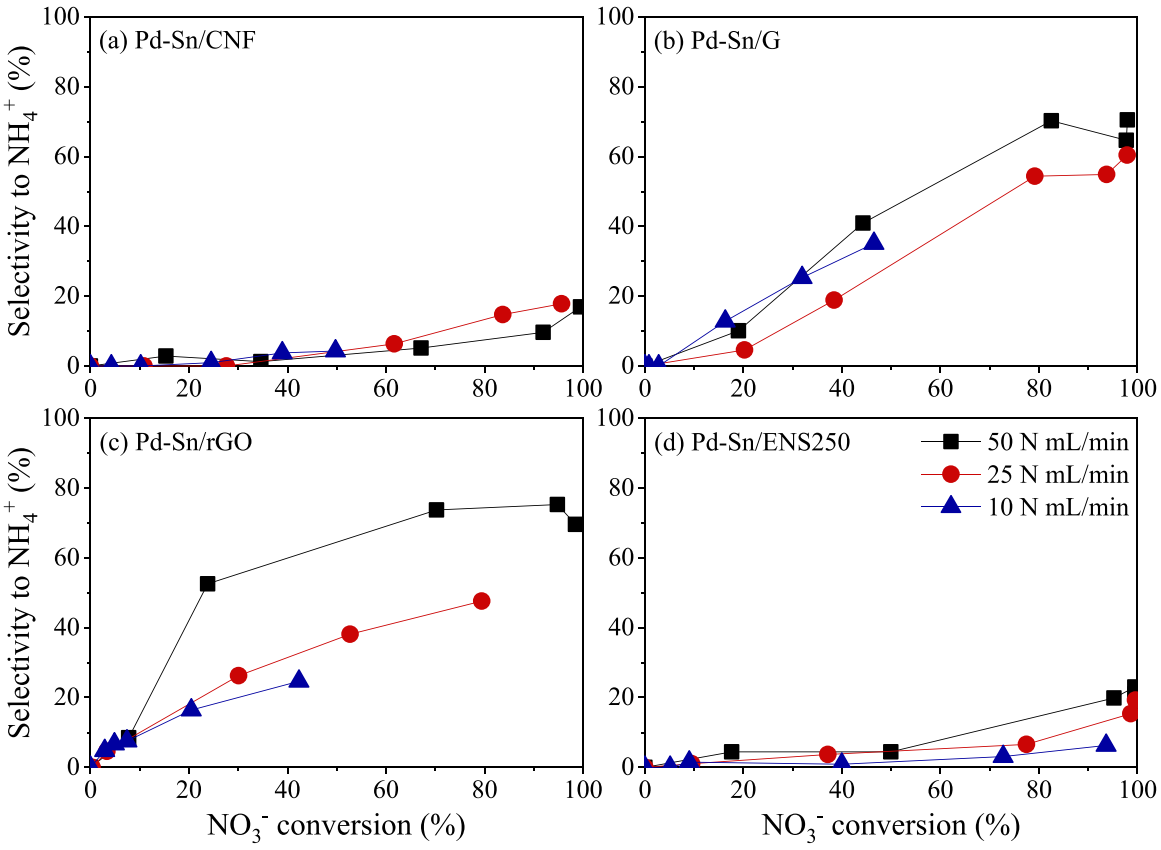


**Fig. 9.** Selectivity to $NH_4^+$ vs $NO_3^-$ conversion for the (a) Pd-Sn/CNF, (b) Pd-Sn/G, (c) Pd-Sn/rGO and (d) Pd-Sn/ENS250 catalysts in FTCMR at different $H_2$ flows ($[NO_3^-]_0$ = 30 mg/L, $CO_2$ flow = 50 N mL/min, 60 mg of catalyst, 30 mm in diameter FTCMR).

However, the activity diminished drastically for those catalysts when $H_2$ flow was reduced from 25 N mL/min to 10 N mL/min, especially for Pd-Sn/CNF and Pd-Sn/G. Regarding Pd-Sn/rGO, the activity reduction was progressive when $H_2$ flow was reduced from 50 N mL/min to 25 N mL/min and 10 N mL/min.

Fig. 9 depicts selectivity to $NH_4^+$ vs $NO_3^-$ conversion for the Pd-Sn/CNF, Pd-Sn/G, Pd-Sn/rGO and Pd-Sn/ENS250 catalysts in the FTCMR. $H_2$ flow decrease did not affect the selectivity to $NH_4^+$ for Pd-Sn/CNF and Pd-Sn/G catalysts. In contrast, $H_2$ flow reduction led to a high decrease in selectivity to $NH_4^+$, especially when $H_2$ flow was reduced from 50 N mL/min to 25 N mL/min for the Pd-Sn/rGO catalyst. Low decrease in selectivity to $NH_4^+$ was observed for the Pd-Sn/ENS250 catalyst. The results indicate that catalysts such as Pd-Sn/CNF and Pd-Sn/ENS250 have a larger operation window as they can be used with higher $H_2$ flow with low impact on selectivity to $NH_4^+$.

## 4. Conclusions

Carbon materials studied in this work as support for Pd-Sn catalysts have shown different physicochemical properties, resulting in diverse performances for $NO_3^-$ reduction and selectivity to $NH_4^+$.

In batch reactor tests, catalyst specific surface area cannot be correlated directly to activity nor selectivity. In this sense, Pd-Sn catalysts with a higher surface area, such as Pd-Sn/AC and Pd-Sn/ENS350, exhibited higher activity in $NO_3^-$ reduction. However, low specific area Pd-Sn/ENS250 catalyst was also very active. In the case of selectivity to $NH_4^+$, low specific surface area Pd-Sn/CNF and Pd-Sn/ENS250 catalysts were less selective to $NH_4^+$, but low specific surface area Pd-Sn/G had a high selectivity to $NH_4^+$. Regarding the promoter metal, Pd-Sn catalysts supported on carbon materials showed similar activity but higher selectivity to $NH_4^+$ than Pd-Cu catalysts when availability of $H_2$ was high. However, Pd-Sn catalysts supported on CNF and ENS250 exhibited selectivity to $NH_4^+$ closer and lower than Pd-Cu ones when $H_2$ flow was decreased, suggesting that Pd-Sn performs better when operating at conditions of gas-liquid mass transfer control.

Lower selectivity to $NH_4^+$ was achieved in the FTCMR for Pd-Sn/CNF, Pd-Sn/AC and Pd-Sn/ENS350 catalysts despite working with higher M/$NO_3^-$ratio, confirming that FTCMR system allows a better control of $H_2$ concentration in the catalytic sites, and that $H_2$ control approach is a feasible way to limit the $NH_4^+$ production of catalysts. The decrease of $H_2$ implies lower conversion, but Pd-Sn/CNF and Pd-Sn/ENS250 where able to work with relatively high $H_2$ flow while maintaining low selectivity to $NH_4^+$.

## CRediT authorship contribution statement

**A. Marí**: Investigation, Writing – original draft, Formal analysis. **J.A. Baeza**: Formal analysis, Writing – review & editing, Validation. **L. Calvo**: Conceptualization, Funding acquisition. **M.A. Gilarranz**: Supervision, Funding acquisition.

## Declaration of Competing Interest

The authors declare that they have no known competing financial interests or personal relationships that could have appeared to influence the work reported in this paper.

## Acknowledgments

The authors greatly appreciate the support from Spanish Agencia Estatal de Investigación (AEI, RTI2018–098431-BI00). Adrián Marí thanks the Spanish AEI for a research grant (PRE-2019–088601).

## Appendix A. Supporting information

Supplementary data associated with this article can be found in the online version at doi:10.1016/j.jece.2022.108011.

## References


[1] O.M. Neijssel, R.R. Meer, K. Luyben, Proceedings 4th European Congress on Biotechnology, 1987, Amsterdam, June 14-19, 1987. In European Congress on Biotechnology 1987: Amsterdam, Netherlands), Elsevier,, 1987.

[2] J.A. Torres-Martínez, A. Mora, J. Mahlknecht, L.W. Daesslé, P.A. Cervantes-Avilés, R. Ledesma-Ruiz, Estimation of nitrate pollution sources and transformations in groundwater of an intensive livestock-agricultural area (Comarca Lagunera), combining major ions, stable isotopes and MixSIAR model, Environ. Pollut. 269 (2021), 115445.

[3] K.D. Vorlop, T. Tacke, Erste schritte auf dem weg zur edelmetallkatalysierten nitrat-und nitrit-entfernung aus trinkwasser, Chemieingenieurtechnik 61 (10) (1989) 836–837.

[4] S. Hörold, T. Tacke, K.D. Vorlop, Catalytical removal of nitrate and nitrite from drinking water: 1, Screen. Hydrog. Catal. Influ. React. Cond. Act. Sel. Environ. Technol. 14 (10) (1993) 931–939.

[5] Directive (EU) 2020/2184 of the European Parliament and of the Council of 16 December 2020 on the quality of water intended for human consumption, ANNEX I: PARAMETERS AND PARAMETRIC VALUES, PART B: Chemical parameters. EUR-Lex. Retrieved 22 April 2021.

[6] Directive (EU) 2020/2184 of the European Parliament and of the Council of 16 December 2020 on the quality of water intended for human consumption, ANNEX I: PARAMETERS AND PARAMETRIC VALUES, PART B: Indicator parameters. EUR-Lex. Retrieved 22 April 2021.

[7] Guidelines for drinking-water quality : fourth edition incorporating the first addendum. Geneva: World Health Organization; 2017. License: CC BY-NC-SA 3.0 IGO.

[8] N. Barrabés, J. Just, A. Dafinov, F. Medina, J.L.G. Fierro, J.E. Sueiras, Y. Cesteros, Catalytic reduction of nitrate on Pt-Cu and Pd-Cu on active carbon using continuous reactor: The effect of copper nanoparticles, Appl. Catal. B: Environ. 62 (1–2) (2006) 77–85.

[9] W. Gao, N. Guan, J. Chen, X. Guan, R. Jin, H. Zeng, F. Zhang, Titania supported Pd-Cu bimetallic catalyst for the reduction of nitrate in drinking water. Appl. Catal. B: Environ. 46 (2) (2003) 341–351.

[10] F.A. Marchesini, S. Irusta, C. Querini, E. Miró, Nitrate hydrogenation over Pt, In/Al2O3 and Pt, In/SiO2. Effect of aqueous media and catalyst surface properties upon the catalytic activity, Catal. Commun. 9 (6) (2008) 1021–1026.

[11] I. Mikami, R. Kitayama, T. Okuhara, Hydrogenations of nitrate and nitrite in water over Pt–promoted Ni catalysts, Appl. Catal. A: Gen. 297 (1) (2006) 24–30.

[12] A. Pintar, J. Batista, I. Musevic, Palladium–copper and palladium–tin catalysts in the liquid phase nitrate hydrogenation in a batch-recycle reactor, Appl. Catal. B-Environ. 52 (2004) 49–60.

[13] N. Krawczyk, S. Karski, I. Witońska, The effect of support porosity on the selectivity of Pd–In/support catalysts in nitrate reduction. Reaction Kinetics, Mech. Catal. 103 (2) (2011) 311–323.

[14] O.S.G. Soares, J.J. Órfão, M.F.R. Pereira, Activated carbon supported metal catalysts for nitrate and nitrite reduction in water, Catal. Lett. 126 (3) (2008) 253–260.

[15] J. Martínez, A. Ortiz, I. Ortiz, State-of-the-art and perspectives of the catalytic and electrocatalytic reduction of aqueous nitrates, Appl. Catal. B: Environ. 207 (2017) 42–59.

[16] A. Pintar, J. Batista, I. Muševič, Palladium-copper and palladium-tin catalysts in the liquid phase nitrate hydrogenation in a batch-recycle reactor, Appl. Catal. B: Environ. 52 (1) (2004) 49–60.

[17] A.E. Palomares, C. Franch, A. Corma, Nitrates removal from polluted aquifers using (Sn or Cu)/Pd catalysts in a continuous reactor, Catal. Today 149 (3–4) (2010) 348–351.

[18] C. Franch, E. Rodríguez-Castellón, Á. Reyes-Carmona, A.E. Palomares, Characterization of (Sn and Cu)/Pd catalysts for the nitrate reduction in natural water, Appl. Catal. A: Gen. 425 (2012) 145–152.

[19] L. Lemaignen, C. Tong, V. Begon, R. Burch, D. Chadwick, Catalytic denitrification of water with palladium-based catalysts supported on activated carbons, Catal. Today 75 (1–4) (2002) 43–48.

[20] T. Yuranova, L. Kiwi-Minsker, C. Franch, A.E. Palomares, S. Armenise, E. García-Bordejé, Nanostructured catalysts for the continuous reduction of nitrates and bromates in water, Ind. Eng. Chem. Res. 52 (39) (2013) 13930–13937.

[21] O.M. Ilinitch, F.P. Cuperus, L.V. Nosova, E.N. Gribov, Catalytic membrane in reduction of aqueous nitrates: operational principles and catalytic performance, Catal. Today 56 (1–3) (2000) 137–145.

[22] Y.X. Chen, Y. Zhang, H.Y. Liu, K.R. Sharma, G.H. Chen, Hydrogen-based tubular catalytic membrane for removing nitrate from groundwater, Environ. Technol. 25 (2) (2004) 227–234.

[23] D.T. González, A. Marí, J.A. Baeza, L. Calvo, M.A. Gilarranz, Enhancement of activity and selectivity to nitrogen in catalytic nitrate reduction by use of conductive carbon catalytic supports and control of hydrogen mass transfer regime, J. Environ. Chem. Eng. (2021), 106419.

[24] H. Takagi, K. Maruyama, N. Yoshizawa, Y. Yamada, Y. Sato, XRD analysis of carbon stacking structure in coal during heat treatment, Fuel 83 (17–18) (2004) 2427–2433.

[25] T. Qiu, J.G. Yang, X.J. Bai, Y.L. Wang, The preparation of synthetic graphite materials with hierarchical pores from lignite by one-step impregnation and their characterization as dye absorbents, RSC Adv. 9 (22) (2019) 12737–12746.

[26] L. Xu, X.C. Wu, J.J. Zhu, Green preparation and catalytic application of Pd nanoparticles, Nanotechnology 19 (30) (2008), 305603.

[27] Y. Gong, P. Zhang, X. Xu, Y. Li, H. Li, Y. Wang, A novel catalyst Pd@ ompg-C3N4 for highly chemoselective hydrogenation of quinoline under mild conditions, J. Catal. 297 (2013) 272–280.

[28] NIST X-ray Photoelectron Spectroscopy Database. http://srdata.nist.gov/xps/ (Retrieved on October 10, 2021).

[29] S.G. Bratsch, Standard electrode potentials and temperature coefficients in water at 298.15 K, J. Phys. Chem. Ref. Data 18 (1) (1989) 1–21.

[30] A.S.G.G. Santos, J. Restivo, C.A. Orge, M.F.R. Pereira, O.S.G.P. Soares, Nitrate Catalytic Reduction over Bimetallic, Catal.: Catal. Optim. C. 6 (4) (2020) 78.

[31] O.S.G.P. Soares, A.G. Gonçalves, J.J. Delgado, J.J.M. Órfão, M.F.R. Pereira, Modification of carbon nanotubes by ball-milling to be used as ozonation catalysts, Catal. Today 249 (2015) 199–203.

[32] F. Rodríguez-Reinoso, The role of carbon materials in heterogeneous catalysis, Carbon 2013 (36) (2013) 159–175.

[33] U. Prüsse, K.D. Vorlop, Supported bimetallic palladium catalysts for water-phase nitrate reduction, J. Mol. Catal. A: Chem. 173 (1–2) (2001) 313–328.

[34] M. D'Arino, F. Pinna, G. Strukul, Nitrate and nitrite hydrogenation with Pd and Pt/SnO2 catalysts: the effect of the support porosity and the role of carbon dioxide in the control of selectivity, Appl. Catal. B: Environ. 53 (3) (2004) 161–168.

[35] J.K. Chinthaginjala, A. Villa, D.S. Su, B.L. Mojet, L. Lefferts, Nitrite reduction over Pd supported CNFs: Metal particle size effect on selectivity, Catal. Today 183 (1) (2012) 119–123.

[36] J.K. Chinthaginjala, L. Lefferts, Support effect on selectivity of nitrite reduction in water, Appl. Catal. B: Environ. 101 (1–2) (2010) 144–149.

[37] Y. Yoshinaga, T. Akita, I. Mikami, T. Okuhara, Hydrogenation of nitrate in water to nitrogen over Pd–Cu supported on active carbon, J. Catal. 207 (1) (2002) 37–45.

[38] M. Al Bahri, L. Calvo, M.A. Gilarranz, J.J. Rodriguez, F. Epron, Activated carbon supported metal catalysts for reduction of nitrate in water with high selectivity towards N2, Appl. Catal. B: Environ. 138 (141–148) (2013).

[39] M.J. Chollier-Brym, R. Gavagnin, G. Strukul, M. Marella, M. Tomaselli, P. Ruiz, New insight in the solid state characteristics, in the possible intermediates and on the reactivity of Pd–Cu and Pd–Sn catalysts, used in denitratation of drinking water, Catal. Today 75 (1–4) (2002) 49–55.

[40] A.H. Pizarro, C.B. Molina, J.J. Rodriguez, F. Epron, Catalytic reduction of nitrate and nitrite with mono-and bimetallic catalysts supported on pillared clays, J. Environ. Chem. Eng. 3 (4) (2015) 2777–2785.

[41] J.J. Carberry, Physico-chemical aspects of mass and heat transfer in heterogeneous catalysis. Catalysis, Springer,, Berlin, Heidelberg, 1987, pp. 131–171.